Ocean Sci. Discuss., 7, 1439–1467, 2010
www.ocean-sci-discuss.net/7/1439/2010/
doi:10.5194/osd-7-1439-2010

Ocean Science Discussions

Flow and mixing around a glacier tongue

C. L. Stevens[1], **C. L. Stewart**[1], **N. J. Robinson**[1,2], **M. J. M. Williams**[1], **and T. G. Haskell**[3]

[1]National Institute for Water and Atmospheric Research (NIWA), Greta Point Wellington, New Zealand
[2]Department of Marine Science, University of Otago, Dunedin, New Zealand
[3]Industrial Research Ltd. (IRL), Gracefield Lower Hutt, New Zealand

Received: 2 August 2010 – Accepted: 3 August 2010 – Published: 11 August 2010

Correspondence to: C. L. Stevens (c.stevens@niwa.cri.nz)

Published by Copernicus Publications on behalf of the European Geosciences Union.

Abstract

A glacier tongue floating in the coastal ocean presents a significant obstacle to the local flow and influences oceanic mixing and transport processes. Here ocean shear microstructure observations at a glacier tongue side-wall show tidally-induced flow pulses and vortices as well as concomitant mixing. Flow speeds within the pulses reached around three times that of the ambient tidal flow amplitude and generated vertical velocity shear as large as $3\times10^{-3}\,s^{-1}$. During the maximum flow period turbulent energy dissipation rates reached a maximum of $10^{-5}\,m^2\,s^{-3}$, around three decades greater than local background levels. This is in keeping with estimates of the gradient Richardson Number which dropped to around unity. Associated vertical diffusivities are higher that expected from parameterization, possibly reflecting the proximity of the cryotopography.

1 Introduction

Quantifying ice–ocean interaction, especially at the small-scale, is proving to be a major challenge in high-latitude earth system sciences (e.g., Sirevaag et al., 2010) where relatively long timescales and complex thermohaline and pressure effects interact with cryogenic topography that is continually changing. Oceanic mixing in polar waters has some differences in drivers and manifestations that at lower latitudes. For example, rotational effects are large, there is little dynamic influence due to temperature, but the effect of being close to the freezing temperature has a controlling influence on behaviour and there are the additional frictional boundary effects of the frozen upper surface (McPhee, 2008).

Glacier (or ice) tongues, formed by glacier outflows into the coastal ocean, can extend many tens kilometers from shore (Frezzotti et al., 1997) and be many hundreds of meters thick in places. Such cryogenic structures significantly influence local circulation and mixing (Jacobs et al., 1981; Legresy et al., 2004). In the case of flow

OSD
7, 1439–1467, 2010

around a glacier tongue, the mixing processes are then combined with the effect of flow around a bluff body. The resulting scales of flow are not normally associated with oceanographic flows with the closest relevant work being that concerning flow around headlands and islands (e.g., Edwards et al., 2004), except of course with a glacier tongue flow can pass under the obstacle.

These ice–ocean interaction processes are important in a situation like southern McMurdo Sound where Haskell Strait forms an oceanic connection between the western Ross Sea and the cavity beneath the combined Ross and McMurdo Ice Shelves (Fig. 1). The Sound acts as a conduit for both ice shelf waters and warmer Ross Sea waters (Robinson et al., 2010). The fate of these waters is dependent on transport and mixing processes in the region. This exchange influences sea ice growth in the region, which in turn affects climate processes over large space and time scales (Hellmer, 2004; Dinniman et al., 2007; Robinson et al., 2010).

The Erebus Glacier Tongue (EGT, Fig. 1) in southern McMurdo Sound has been observed to influence local vertical stratification (Jacobs et al., 1981) through formation of diffusive-convective layering. It has also been suggested that such glacier/ice tongues generate local sources of supercooled water (e.g., Debenham, 1965; Jeffries and Weeks, 1992) – water cooled at depth to the in situ freezing temperature but then advected to shallower depths where it is colder than the new insitu freezing point. In the absence of nucleation centers, this supercooled water remains liquid or forms frazil/platelets (e.g., Dmitrenko et al., 2010). Such properties are readily observed in the region (Gough et al., 2010; Robinson, 2010) including during the very first of such observations in 1911 (Deacon, 1975).

The EGT thus provides an ideal site to examine the degree of variability of, and interaction between, small-scale mixing and advective processes. Much work has been developed relating to the cryomechanics and the effect of the ocean on the glacier tongue (see Squire et al., 1994 and papers therein). As well as providing evidence for the effect of the glacier tongue on local oceanography, the present data also have relevance for flow and melting processes at the face of ice shelves (Rignot et al., 2010).

OSD
7, 1439–1467, 2010

The objective here is to present new microstructure observations providing evidence of mixing rates at the tip of a glacier tongue, paying special attention to (i) water column structure and kinematics, (ii) mixing, (iii) mechanisms for enhancement of local supercooling and (iv) generalization of the results beyond the EGT.

2 Methods

2.1 Location

In November 2009 we conducted oceanographic measurements within 30 m of the sidewall of the EGT which divides the surface waters of the majority of Erebus Bay from the Dellbridge Islands and Cape Evans (Fig. 1c). At the time of sampling the glacier tongue was 12 km long, 2.5 km wide and 300 m thick at the grounding line, and with a basal slope of around 0.02 along its main axis, and the tip is around 50 m thick (Debenham, 1965; Holdsworth, 1982; DeLisle et al., 1989). Water depths near its tip are around 400 m (Jacobs et al., 1981) but highly variable due to the geology of the region including likely moraine deposits (Fig. 1d). At the time of writing the most recent calving of the EGT was in March of 1990 when a 3.5 km section broke away. Similar events were known to have occurred in 1911 and at some point during the 1940s (Robinson and Haskell, 1990).

Available data on near-surface residual circulation are sparse but suggest a predominant northward current near the south of Erebus Bay (Fig. 1c), at least during winter (Leonard et al., 2006; Robinson, 2010; Mahoney et al., 2010). Tidal flows some 5 km to the SW of the EGT reached amplitudes of around 0.15 m s^{-1} (Stevens et al., 2006).

2.2 Instrumentation

A 300 kHz acoustic Doppler current profiler (ADCP-RDI Workhorse) was deployed through a hole in the 2.3 m thick first year fast-ice for a four day period (Fig. 1c) around

OSD
7, 1439–1467, 2010

1 km shoreward from the tip on the north side of the EGT (Fig. 1d). The ADCP was held just beneath the sea ice (i.e. 2.5 m) with the first measurements starting 4 m below this. The sampling recorded 2 m thick velocity bins every 5 min. Good quality data was typically resolved down to depths of 120 m. This is quite good penetration for this type of instrument in these waters where we have had far shallower penetration due to lack of suitable scatterers (Leonard et al., 2006; Stevens et al., 2006). A magnetic declination offset of 146 degrees was included. Compass testing did not indicate any inconsistencies due to the near-vertical magnetic field. Tidal elevation data were recorded at Scott Base near Cape Armitage, 17 km to the south.

Turbulence properties were resolved with a Rockland VMP500 microstructure loose-tethered free-fall profiler with dual shear sensors (Macoun and Lueck, 2004) with the key property being the turbulent energy dissipation rate ε (units of $m^2\,s^{-3}$ equivalent to $W\,kg^{-1}$). Thirty eight profiles were recorded with a total profiled distance of over 11 km. The profiles penetrated to around 300 m depth, although only the upper 120 m are considered here as the focus is on the EGT effect and the comparison with the ADCP. Energy dissipation rates (ε) were resolved from the dual shear probe profiler (Prandke, 2005; Roget et al., 2006) and the data revealed a noise floor in terms of ε of around $3\times10^{-10}\,m^2\,s^{-3}$. In addition, a SBE (Seabird Electronics, USA) temperature and conductivity sensor pair were mounted on the VMP500. These sensors are unpumped so as to not affect the shear data through the creation of spurious vibrations, so the spatial resolution is around 1 m. The profiler was kept in the water continuously so that it was at the ambient temperature removing thermal inertia start-up effects. The turbulence data do not have a continuous temporal coverage due to operational constraints and so there were a number of gaps in the profiling, most notably a 2.5 h gap, fortunately during a period of slower flow.

The microstructure data were separated into 5 m bins that were overlapped by 50%. Dissipation rates, velocities and scalar properties were all interpolated onto this depth scale to enable calculation of a number of derived quantities. Sorting the profile into a statically stable profile generates a displacement lengthscale. Cumulatively summing

OSD
7, 1439–1467, 2010

these displacements resolves overturning scales described by the Thorpe overturn lengthscale L_T (Roget et al., 2006).

3 Observations

The largely diurnal tides in the region are around 1 m in peak-peak elevation (Goring and Pyne, 2003) with a 14 day "spring-neap" cycle (Fig. 2a). While these tides typically generate maximum flows of 15 cm s^{-1} in the Sound-proper (Leonard et al., 2006; Stevens et al., 2006; Robinson, 2010), here we saw flow magnitudes reach 40 cm s^{-1} (Fig. 2c). The currents appear cyclical (Fig. 2c) but careful examination reveals the faster flows in each cycle were not phase-locked to the tide. The short duration of the dataset precluded any co-spectral analysis. The weak South-east flow at the low tide was the most consistent feature. The faster flow on the rising/high tide was more variable especially in its direction. The strongest flow was quite short in duration in each tidal period and so we refer to it here as a pulse, in an otherwise moderately quiescent water column.

A diurnal cycle of concurrent turbulence and ADCP data (day of year 323.6–324.6; i.e. 20–21 November 2009) is the focus here (Fig. 3) – coincidentally this was the diurnal period during which the strongest measured pulse-like flow occurred (Fig. 2). The pulse was located on the rising phase of the tide and, at the observation point at least, this was seen as flow acceleration initially at depths >40 m at which time shallower flows were towards the EGT suggesting a wake recirculation in the vertical. The pulse then deepened to fill the entire measured depth before decaying. The main body of the pulse lasted around 4 h. It was followed by some wave-like "ringing" (using an acoustic analogy) whereby there were moderate flow accelerations for short periods spaced a little over an hour apart. Directionally the pulse, including its trailing ringing, moved mainly eastward. The flow preceding the pulse was directed around 180 degrees from this, heading W whilst the flow directly after the ringing was to the north-NW. Flows other than during the pulse were relatively weak but still a moderate

OSD
7, 1439–1467, 2010

proportion of the tidal amplitude observed at locations away from the coast (Leonard et al., 2006; Stevens et al., 2006; Robinson, 2010). These horizontal pulse flows were accompanied by relatively strong vertical flows that reached up to 10 cm s^{-1} (Fig. 3b). The main body of the pulse generated upwards flow at the sampling position. However, the post-pulse ringing contained both up and down flows.

Backscatter amplitude variations as seen here (Fig. 3e) often provide a qualitative picture of a tracer field (Leonard et al., 2006; Stevens et al., 2006). It is a difficult property to interpret as it is an integral whereby the value at a given depth is a function of the water column through which the acoustic beams must pass twice. Hence, a low acoustic backscatter at say 80 m might indicate few reflectors at that depth or a high degree of flow attenuation above the sample volume. There were three periods in the 24 h when the backscatter was reduced sufficiently enough to affect the velocity signal to noise ratio adversely so that the deepest depth of good quality data would shoal. These reductions were pre- and post-pulse, as well as a sustained period occurring 12 h after the pulse. This might be a diurnal cycle in scattering due to biological modulation as, despite the 24 h daylight, a variation in signal can persist in the region (A. Mahoney, personal communication; Leonard et al., 2010). Our sampling coincided with a period when the pulse was essentially around midnight local time so it was co-located temporally with what should be biologically-induced maximum penetration. Furthermore, this diurnal variation was not nearly as strongly apparent on other days. Thus, the drop in backscatter may have been a response entirely to the stronger flow. Curiously, at the very end of the data shown in Fig. 3e there was a period when there was a local minimum in backscatter between 20 and 40 m depth. This effect was not seen in earlier measured tidal periods when the flow was weaker.

Velocity shear S was resolved from the vertical derivative of horizontal velocity components u and v (east-west and north-south, respectively) so that

$$S = \left[\left(\frac{\partial u}{\partial z} \right)^2 + \left(\frac{\partial v}{\partial z} \right)^2 \right]^{1/2}.$$

OSD
7, 1439–1467, 2010

This was typically in the order of $5\times10^{-4}\,s^{-1}$, although during the main pulse flow it reached six times this value i.e. $3\times10^{-3}\,s^{-1}$ (Fig. 3d). At the same time, the stratification (Fig. 3f) persisted during the strongest section of the pulse flow. The buoyancy frequency squared is calculated from the vertical derivative of density $\partial\rho/\partial z$ so that

$$N^2 = \frac{g}{\rho_0}\frac{\partial\rho}{\partial z}$$

where ρ_0 is a reference (background) density and g is gravitational acceleration.This was greatest during and just after the pulse flow (Fig. 3f) when lighter fluid appeared in the upper 40 m of the water column and N^2 reached $10^{-5}\,(\mathrm{rad\,s^{-1}})^2$. During the period after the pulse and ringing N^2 was at detectable limits of around $10^{-8}\,(\mathrm{rad\,s^{-1}})^2$. These values bracket other observations in the Sound (Stevens et al., 2009) where $3\times10^{-6}\,(\mathrm{rad\,s^{-1}})^2$ was observed around the topography of the ridge running off Cape Armitage.

The turbulent energy dissipation rate ε reached a maximum of $10^{-5}\,m^2\,s^{-3}$ (Fig. 3h). Such high dissipation rates were mostly confined to the upper 40 m of the measured water column for a period of around four hours. The ringing was aliased in the profiling so that any elevated ε associated with these brief accelerations was not necessarily captured. After the ringing had finished the ε dropped to levels around $10^{-7}\,m^2\,s^{-3}$ and then, after the final backscatter minimum (time 324.5; midday 21 November 2009), it fell to the noise floor of the instrument at a little above $10^{-10}\,m^2\,s^{-3}$.

A single example microstructure profile (Fig. 4) from around the time of maximum dissipation rate (time=323.95) showed that the temperature was around 0.1 °C above freezing and so supercooling was not apparent or indeed likely. However, evidence from other years suggests this is not the case every year (Fig. 6) and certainly at other times of the year there is much more substantial variation in temperature in the ambient fluid (Mahoney et al., 2010). The microstructure example of Fig. 4 was chosen as it contained the highest dissipation rates and, of all the profiles, it most strongly suggested the influence of the base of the EGT with strong steps in properties at

OSD
7, 1439–1467, 2010

50 and 100 m. The salinity (and hence density, as it follows salinity very closely at such temperatures) exhibited an unusual local minimum at 50 m. Potentially this was surface or near-wall fluid swept to the base of the EGT by vortices. This generates some large scale structure in the Thorpe overturning scale L_T in the upper part of the water column. However, as the profile do not go all the way to the bed, deeper values of this measure are possible so that this is a lower bound as there is a large-scale overturn that results in the heaviest water in the partial profile being located at a depth of 108 m. Considering the L_T distribution over the entire experiment (Fig. 5), the deeper large overturn is seen to be the largest recorded. The pulse was preceded by a strong overturn of around 70 m (at time 323.8). During the pulse and ringing period the upper water column consisted mainly of overturns in the 0–20 m range as seen in the Fig. 4 example. After the ringing had ceased (324.2), there was a relatively large period of 70 m overturns which then fell away to 40 m or less.

4 Discussion

4.1 Kinematics and water column structure

One naïve expectation that was dispelled by the observations was that the local maximum depth of the EGT would be consistently clear in the data, either through a step in stratification or a strongly consistent velocity shear feature. That these were not apparent is probably indicative of the fact that the underside of the glacier tongue is not level either along, or across, its main longitudinal axis (Holdsworth, 1982). Even the relatively weak local stratification will retard vertical flows, so that the influence of the glacier tongue closer to the grounding line might still have a strong influence at the observation position thus spreading the depth of the effect on properties.

In the case of the EGT flow, the so-called ringing was comprised of accelerations around 70 min apart. Presumably, this marks either a wave or vortex process as the flow accelerates during the pulse. The 70 min period doesn't particularly fit any kind

OSD
7, 1439–1467, 2010

of local seiche across to Tent Island, being too slow and too fast for barotropic and baroclinic waves, respectively (see Albrecht et al., 2006 for a description of baroclinic timescale in the region). Of course, the waves could be associated with a different boundary.

There is some evidence for the ringing response being associated with shed vorticies. Certainly the L_T at this time was comparable to the local depth of the EGT (Fig. 5). Consideration of rotational velocity spectra both near the surface and deeper (Fig. 7) do not yield any strong differences associated with direction of rotation except for (i) a weak emphasis on clockwise motion at lower frequencies and (ii) a significant difference at around 20 cpd. This latter difference might be associated with the "ringing" timescale seen in the ADCP data (Fig. 3). When comparing spectra from the two depths, the only obvious difference is the different slopes in the 1–24 cpd bands, with the deeper data exhibiting a shallower slope. This suggests there is greater energy finding a pathway through the internal wave spectrum beneath the tongue. This is entirely feasible as (i) the fast ice boundary potentially generates a more homogenous surface layer less able to support internal waves and (ii) internal waves persist at depths other than that at which the obstacle exists (e.g. mountain lees waves).

The Strouhal number $St=fL/u$ (f is shedding frequency, L is lengthscale and u is velocity) is in the range 0.03–0.3 (assuming $f=2\times10^{-4}\,s^{-1}$, $L=50$–$500\,m$ and $u=0.3\,m\,s^{-1}$). This intermediate flow regime suggests variable flow with buildup and release of vorticies (Sobey, 1982). Thus, on the inward flood tide into the Dellbridge Islands embayment, vorticies are likely shed off the tip of the EGT as supported by the clockwise spectral energy. Headland studies (Edwards et al., 2004) have demonstrated the effectiveness of spatial mapping of currents. However, such mapping is difficult in the presence of fast ice requiring autonomous vehicle technology (e.g., Hayes and Morison, 2002).

Not only does melting of glacier and ice shelf walls have a strong influence on the ice dynamics (Rignot et al., 2010; Olbers and Hellmer 2010), it can also result in highly variable stratification near the wall, including double diffusive layering (Jacobs et al.,

OSD
7, 1439–1467, 2010

1981). Whilst the present study was initially motivated by the search for diffusive convection as observed in the Jacobs study, it is beyond the scope of the present work to compare the magnitudes of shear-induced and diffusion-induced mixing as we have no complementary observations of the latter situation. It seems highly likely that the pulse feature would sweep away layering structure generated by double diffusion. However, the pulse is transient and so for the majority of the time conditions were relatively quiescent and thus conducive to the accumulation of meltwater. Hence, further exploration of the melting processes needs to incorporate temporal variation in the ambient conditions at timescales far less than a tidal period.

4.2 Mixing rates

The energy dissipation rate (ε) rose – albeit for localized moments in time and presumably space – as much as three orders of magnitude above what might be regarded as normal background levels. Edwards et al. (2004) noted how local turbulent buoyancy flux scaled with ε and that it is likely maximum very close to a headland. Present modeling (Dinniman et al., 2007; Reddy et al., 2010) that encompasses the region is at a scale that is unlikely to be instantaneously influenced even by this degree of variability. However, as seen in benthic observations to the north of McMurdo Sound (Muench et al., 2009), over long timescales the continual focus of high energy dissipation rates and concomitant enhance diffusivities suggest that such processes and scales are important. Intermediate scales of regional modeling would elucidate this influence.

In order to parameterize the likelihood of instability and mixing, the gradient Richardson Number,

$$Ri_{\mathrm{gr}} = \frac{N^2}{S^2},$$

a measure of shear-induced instability whereby values substantially less than unity are likely to be or become unstable, can be calculated. The flow observed here is rather

OSD
7, 1439–1467, 2010

intermittent as it is the ratio of two derivative properties so that noise and uncertainty is amplified. However, the depth-time distribution of Ri_{gr} does have some consistent structure (Fig. 8) so that in the core of the pulse $Ri_{gr}<1$, implying mixing due to shear is likely and this was borne out by the dissipation rate observations. At times away from the pulse feature, stratification persisted more strongly so that $N^2=10^{-5}\,(\mathrm{rad\,s^{-1}})^2$ and background shear was more like $S^2=3\times10^{-8}\,\mathrm{s^{-2}}$. Under these conditions $Ri_{gr}=100$, implying mixing was unlikely.

Efforts continue to determine the functionality of vertical mixing in response to the balance captured in Eq. (1) (e.g., Zaron and Moum, 2009). Fer (2006) suggests modification of the Pacanowski and Philander (1981) formulations for vertical diffusivities of momentum and buoyancy (K_m and K_ρ). These modifications, based on observations in an Arctic Fiord and so likely relevant here, are given as

$$K_m = \frac{5.5\times10^{-3}}{(1+5Ri_{gr})^2} + K_{m0}$$

$$K_\rho = \frac{K_m}{(1+5Ri_{gr})} + K_{\rho 0}$$

where background levels are given by $K_{m0}=1.3\times10^{-3}\,\mathrm{m^2\,s^{-1}}$ and $K_{\rho 0}=1.3\times10^{-4}\,\mathrm{m^2\,s^{-1}}$. There are trends between the estimate of the Ri_{gr} and the measured dissipation and inferred vertical diffusivity K_ρ (Fig. 9). The diffusivity is somewhat higher than the model determined by Fer (2006) – especially in the $Ri_{gr}=1$–10 band. There is an important point here though. The K_ρ estimates presented here use the Shih et al., 2005 estimate for K_ρ which are, like the comparison made in Stevens et al. (2009), somewhat higher than the Osborne method for estimating K_ρ. However, the Fer (2006) model uses the Osborn model which it notes is an upper bound (see Zaron and Moum, 2009). The discrepancy possibly lies in the likely small scales in forcing. The observed N^2 may not be particularly representative of the conditions that spawned the mixing. It is useful to consider the relationship between

OSD
7, 1439–1467, 2010

displacement and energy dissipation. Assuming a timescale of 8 min associated with an N^2 of 2×10^{-4} $(\mathrm{rad\,s^{-1}})^2$ then placing dissipation rate estimates on a displacement diagram it is clear that the eastward flowing periods generated the strongest dissipation rates and the scales of the "action at a distance" were comparable with the distance to the tip of the glacier tongue. Thus, the observations downstream might be the result of direct flow-obstacle interaction.

4.3 Local supercooling

A number of authors have inferred that glacier/ice tongues might be generators of supercooled water (Debenham, 1965; Jeffries and Weeks, 1992). Such conditions arise when seawater in contact with ice at depth is cooled to the in situ freezing point. If, at some later time it rises in the water column, the increase in local freezing temperature may result in the fluid actually being colder than this temperature. This substantially increases it's propensity to freeze. While this is unlikely in the particular relatively warm period observed here, there have been previous times even at the same time of year when it has been possible as shown in CTD data of Fig. 6. Thus, the presently observed kinematics are relevant to the supercooling problem. The ADCP data do show a weak upward flow for most of the time. Furthermore, as the post-pulse "ringing" has a half-period timescale of 35 min and a vertical speed of around $0.05\,\mathrm{m\,s^{-1}}$ then the individual events might be expected to advect water around 100 m vertically in this time.

Platelet growth rates are very difficult to quantify as they inherently depend on their initial conditions and observations have difficulty in separating advection versus actual growth. However, Leonard et al. (2006) observed 30 cm cylinders of platelets growing on near-surface lines after periods as short as three days. Consequently if, as in the EGT situation, water advected up from beneath the tongue were immediately returned to depth it is unlikely there would be any effect. If, on the other hand, the flow were rectified in some way which is likely given the non-linearity of the "flow around headland" mechanics, this displacement represents a $-0.075\,^{\circ}\mathrm{C}$ change in the freezing point and

OSD
7, 1439–1467, 2010

so highly influential if the local water is very cold. Similar temporally variable generation possibilities exist in the internal waves observed at Cape Armitage 17 km to the south of the EGT (Robinson, 2010).

4.4 Generalization

Sharp headlands strongly influence local flow through rectification of tides (e.g., Edwards et al., 2004). Although the EGT's finger-like morphology is at the extreme end of the headland aspect ratio scale and glacier tongues are located at the surface rather than the bed we expect there is much in common in terms of oceanic response to tidal flow. The headland work of Edwards et al. (2004) identified the split between skin and form drag and that the majority of the diapycnal turbulent buoyancy flux occurred close by the headland.

The EGT has quite a large aspect ratio (length/width) when compared to the Drygalski Ice Tongue (and the Mertz and Ninnis Glacier Tongues prior to their recent break ups). At the same time, the EGT is smaller in absolute scale by a factor of ten from these giant glacier tongues. Possibly the EGT is atypical in that it is protected from currents and waves by the Dellbridge Islands and also the generally low tidal flows in the area.

A subjective series of sketches (Fig. 11) shows the likely flow evolution around the EGT. The tidally-driven flow is highly rectified and also variable with depth and so generates quite specific mixing events in time and presumably space. It would be useful to translate this description to other systems.

Consequently, the relative scale of separated flow to that of the tongue is likely much larger with the EGT. However, vertical scales are greater for the big ice tongues so that vertical flows may be even stronger. Where the present data are of relevance to both the larger ice tongues and indeed ice shelf fronts is at the small scale. The data demonstrate the small temporal scales of variability in turbulence, the strong and fluctuating vertical flows, and the very large dissipation rates and diffusivities possible right next to the ice wall.

OSD
7, 1439–1467, 2010

Acknowledgements. The authors wish to thank Pat Langhorne, Andy Mahoney, Alex Gough, Robin Robertson and Melissa Bowen for useful discussions associated with this work. Brett Grant, Stéphane Popinet, David Plew, Brian Stait and Peter Gerring assisted with field work. Funding and support were provided by The New Zealand Royal Society administered Marsden Fund, Antarctica New Zealand (Events K131/K132) and the New Zealand Foundation for Research Science and Technology (Contract C01X0701). This paper is dedicated to the memory of Don Lewis.

References

Albrecht, N., Vennell, R., Williams, M., Stevens, C., Langhorne, P., Leonard, G., and Haskell, T.: Observation of sub-inertial internal tides in McMurdo Sound, Antarctica, Geophys. Res. Lett., 33, L24606 doi:10.1029/2006GL027377, 2006.

Deacon, G. E. R.: The oceanographic observations of Scott's last expedition, Polar Rec., 17, 391–419, 1975.

Debenham, F.: The glacier tongues of McMurdo Sound, Geogr. J., 131, 369–71, 1965.

DeLisle, G., Chinn, T., Karlen, W., and Winters, P.: Radio echosounding of Erebus Glacier Tongue, New Zealand Antarctic Record, 9, 15–30, 1989.

Dinniman, M. S., Klinck, J. M., and Smith, Jr., W. O.: Influence of sea ice cover and icebergs on circulation and water mass formation in a numerical circulation model of the Ross Sea, Antarctica, J. Geophys. Res., 112, C11013, doi:10.1029/2006JC004036, 2007.

Dmitrenko, I. A., Wegner, C., Kassens, H., Kirillov, S. A., Krumpen, T., Heinemann, G., Helbig, A., Schröder, D., Hölemann, J. A., Klagge, T., Tyshko, K. P., and Busche, T.: Observations of supercooling and frazil ice formation in the Laptev Sea coastal polynya, J. Geophys. Res., 115, C05015, doi:10.1029/2009JC005798, 2010.

Edwards, K., MacCready, P., Moum, J., Pawlak, G., Klymak, J., and Perlin, A.: Form drag and mixing due to tidal flow past a sharp point, J. Phys. Oceanogr., 34, 1297–1312, 2004.

Emery, W. J. and Thomson, R. E.: Data Analysis Methods in Physical Oceanography, Pergamon, 634 pp., 1997.

Fer, I.: Scaling turbulent dissipation in an Arctic fjord, Deep-Sea Res. Pt. II, 53, 77–95, 2006.

Frezzotti, M.: Ice front fluctuation, iceberg calving flux and mass balance of Victoria Land Glaciers, Antarct. Sci., 9, 61–73, 1997.

OSD

7, 1439–1467, 2010

Gough, A. J., Mahoney, A., Langhorne, P. J., Williams, M. J. M., Stevens, C. L., and Haskell, T. G.: Supercooling and seeding: oceanographic disruption of preferred crystal orientation in sea ice growing near ice shelves, IAHR Proceedings 20th IAHR International Symposium on Ice, Helsinki, 2010.
Goring, D. G. and Pyne, A.: Observations of sea-level variability in Ross Sea, Antarctica, New Zeal. J. Mar. Fresh., 37, 241–249, 2003.
Hayes, D. R. and Morison, J. H.: Determining turbulent, vertical velocity, and fluxes of heat and salt with an autonomous underwater vehicle, J. Atmos. Ocean. Tech., 19, 759–779, 2002.
Hellmer, H. H.: Impact of Antarctic ice shelf basal melting on sea ice and deep ocean properties, Geophys. Res. Lett. 31, L10307, doi:10.1029/2004GL019506, 2004.
Holdsworth, G.: Dynamics of Erebus Glacier tongue. Ann. Glaciol., 3, 131–137, 1982.
Jacobs, S. S., Huppert, H. E., Holdsworth, G., and Drewry, D. J.: Thermohaline steps induced by melting of the Erebus Glacier Tongue, J. Geophys. Res., 86, C7, 6547–6555, 1981.
Jeffries, M. O. and Weeks, W. F.: Structural characteristics and development of sea ice in the Western Ross Sea, Antarct. Sci., 5(1), 63–75, 1992.
Legresy, B., Wendt, A., Tabacco, I., Remy, F., and Dietrich, R.: Influence of tides and tidal current on Mertz Glacier, Antarctica, J. Glaciol., 50, 427–435, 2004.
Leonard, G. H., Purdie, C. R. Langhorne, P. J., Haskell, T. G., Williams, M. J. M., and Frew, R. D.: Observations of platelet ice growth and oceanographic conditions during the winter of 2003 in McMurdo Sound, Antarctica, J. Geophys. Res., 111, C04012, doi:10.1029/2005JC002952, 2006.
Leonard, G. H., Purdie, C. R., Langhorne, P. J., Williams, M. J. M., and Haskell, T. G.: Ice crystals in the water column: the view from an Acoustic Doppler Current Profiler (ADCP), IAHR Proceedings 20th IAHR International Symposium on Ice, Helsinki, 2010.
Macoun, P. and Lueck, R. G.: Modelling the spatial response of the air-foil shear probe using different sized probes, J. Atmos. Ocean. Tech., 21, 284–297, 2004.
Mahoney, A., Gough, A., Langhorne, P., Robinson, N., Stevens, C., Williams, M., and Haskell, T.: The seasonal arrival of ice shelf water in McMurdo Sound and its effect on sea ice growth, in preparation, 2010.
McPhee, M. G.: Air-Ice-Ocean-Interaction: Turbulent Ocean Boundary Layer Exchange Processes, Springer, 215 pp., 2008.
Muench, R., Wåhlin, A., Özgökmen, T., Hallberg, R., and Padman, L.: Impacts of bottom corrugations on a dense Antarctic outflow: the NW Ross Sea, Geophys. Res. Lett., 36, 23,

OSD
7, 1439–1467, 2010

doi:10.1029/2009GL041347, 2009.
Olbers, D. and Hellmer, H.: A box model of circulation and melting in ice shelf caverns, Ocean Dynam., 60, 141–153, doi:10.1007/s10236-009-0252-z, 2010.
Pacanowski, R. C. and Philander, S. G. H.: Parameterization of vertical mixing in numerical models of tropical oceans, J. Phys. Oceanogr., 11, 1443–1451, 1981.
Prandke, H.: Microstructure sensors, in: Marine Turbulence: Theories, Observations and Models, edited by: Baumert, H. Z., Simpson, J. H., and Sundermann, J., Cambridge Univ. Press, 101–109, 2005.
Reddy, T. E., Holland, D. M., and Arrigo, K. R.: Ross ice shelf cavity circulation, residence time, and melting: results from a model of oceanic chlorofluorocarbons, Cont. Shelf Res., 30, 733–742, doi:10.1016/j.csr.2010.01.007, 2010.
Rignot, E., Koppes, M., and Velicogna, I.: Rapid submarine melting of the calving faces of West Greenland Glaciers, Nat. Geosci., 3, 187–191, doi:10.1038/ngeo765, 2010.
Robinson, W. and Haskell, T. G.: Calving of Erebus Glacier tongue, Nature 346, 615–616. 1990.
Robinson, N. J., Williams, M. J. M., Barrett, P. J., and Pyne, A. R.: Observations of flow and ice–ocean interaction beneath the McMurdo Ice Shelf, Antarctica, J. Geophys. Res., 115, C03025, doi:10.1029/2008JC005255, 2010.
Robinson N. J.: The ocean boundary layer beneath Antarctic Sea ice in the vicinity of an ice shelf, Ph.D. Thesis, Univ. Otago, 2010.
Roget, E., Lozovatsky, I., Sanchez, X., and Figueroa, M.: Microstructure measurements in natural waters: methodology and applications, Progr. Oceanogr., 70, 126–148, 2006.
Shih, L. H., Koseff, J. R., Ivey, G. N., and Ferziger, J. H.: Parameterization of turbulent fluxes and scales using homogeneous sheared stably stratified turbulence simulations, J. Fluid Mech., 525, 193–214, 2005.
Sirevaag, A., McPhee, M. G., Morison, J. H., Shaw, W. J., and Stanton, T. P.: Wintertime mixed layer measurements at Maud Rise, Weddell Sea, J. Geophys. Res., 115, C02009, doi:10.1029/2008JC005141, 2010.
Squire, V. A., Robinson, W. H., Meylan, M., and Haskell, T. G.: Observations of flexural waves on the Erebus Ice Tongue, McMurdo Sound, Antarctica, and nearby sea ice, J. Glaciol., 40, 377–385, 1994.
Sobey, I. J.: Oscillatory flows at intermediate Strouhal number in asymmetric channels, J. Fluid Mech., 125, 359–373, 1982.

OSD
7, 1439–1467, 2010

Stevens, C. L., Robinson, N. J., Williams, M. J. M., and Haskell, T. G.: Observations of turbulence beneath sea ice in southern McMurdo Sound, Antarctica, Ocean Sci., 5, 435–445, doi:10.5194/os-5-435-2009, 2009.

Stevens, C. L., Williams, M. J. M., Robinson, N. J., Albrecht, N., and Haskell, T. G.: Observations of the stratified turbulent boundary-layer and platelet ice beneath McMurdo Sound Sea Ice, Proc. Sixth International Symposium on Stratified Flows, edited by: Ivey, G. N., Perth, Australia, 2006.

Zaron, E. D. and Moum, J. N.: A new look at Richardson Number mixing schemes for equatorial ocean modeling, J. Phys. Oceanogr., 39(10), 2652–2664, 2009.

OSD

7, 1439–1467, 2010

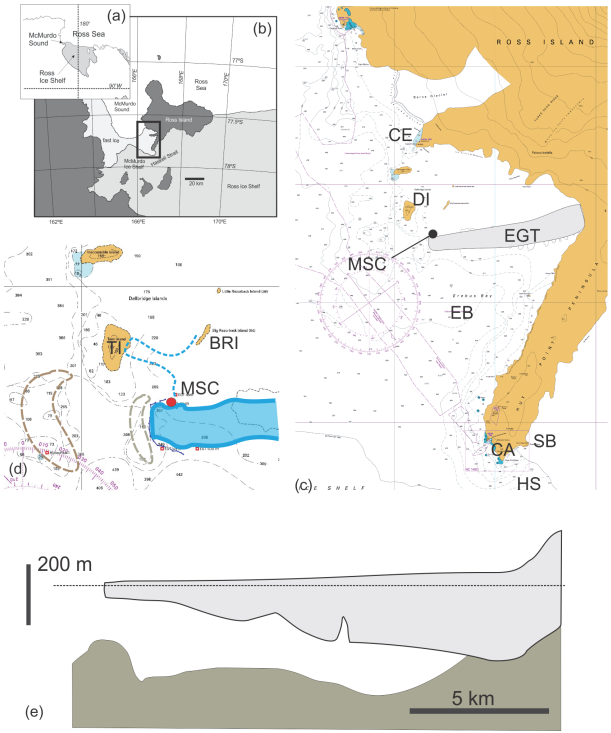

Fig. 1. (a) McMurdo Sound located in the South Western Ross Sea near **(b)** the McMurdo and Ross Ice Shelves. **(c)** The Erebus glacier tongue station (EGT) and the complex topography of the Dellbridge Islands (DI) are marked relative to Erebus Bay (EB), Cape Evans (CE). Cape Armitage (CA), Haskell Strait (HS) and Scott Base (SB). The microstructure field camp (MSC) **(d)** was around 1000 m east of the tip of the EGT. The grey lines highlight known bathymetric features whilst the blue dashed line shows a tongue of multi year fast ice extending out to Tent Island (TI) and Big Razorback Island (BRI). Map excerpt courtesy of Land Information New Zealand. **(e)** A cross-section of the EGT simplified from DeLisle et al. (1989).

OSD
7, 1439–1467, 2010

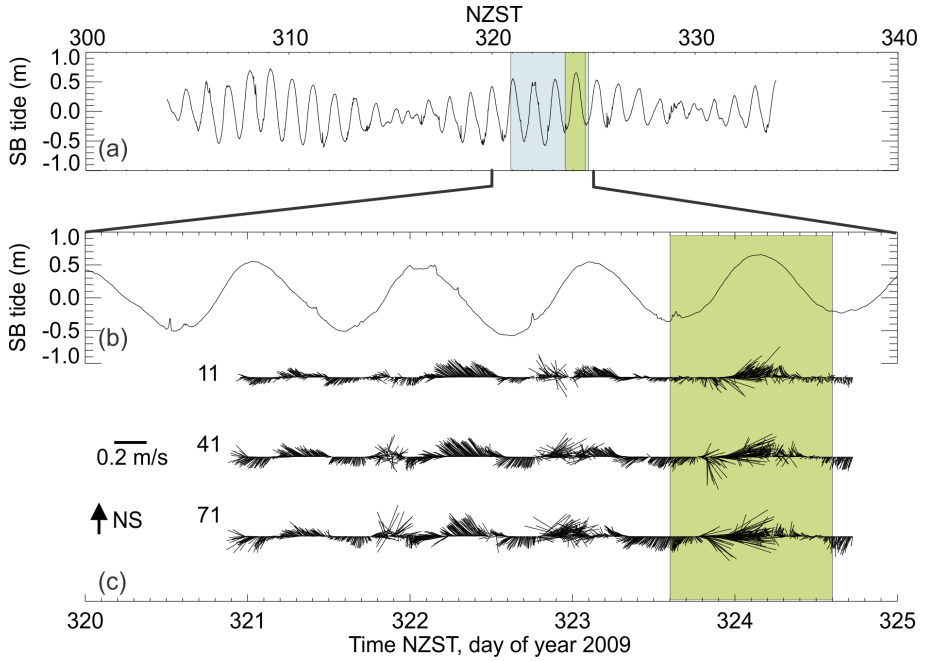

Fig. 2. The tidal elevation **(a)** at Scott Base is expanded **(b)** to highlight a five day segment within which our **(c)** ADCP (grey box in a) and turbulence profiling (green box in all panels) were recorded. Panel **(c)** shows velocity feather vectors for 3 depth bins centered at 11, 41 and 71 m.

OSD
7, 1439–1467, 2010

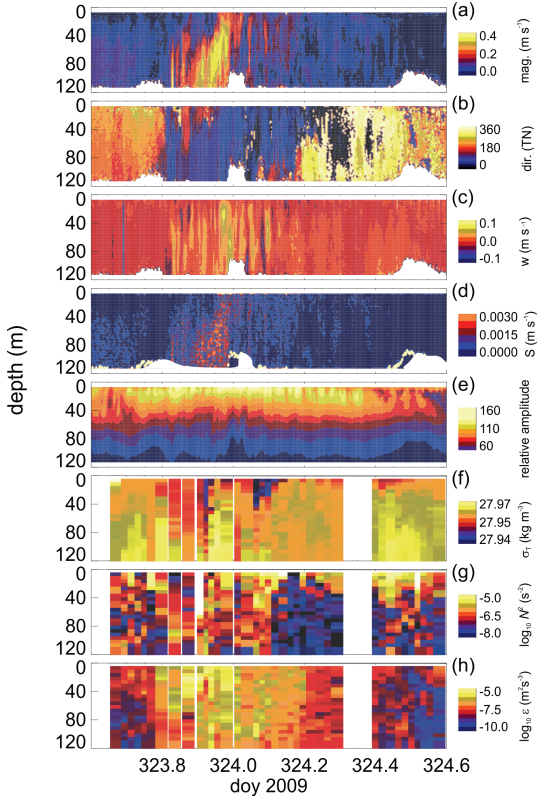

Fig. 3. ADCP and turbulence data products. The ADCP resolved **(a)** horizontal velocity magnitude, **(b)** horizontal direction in which the flow is going, **(c)** vertical velocity w, **(d)** vertical shear and **(e)** backscatter amplitude. The VMP turbulence profiler resolved **(f)** density as σ_t, **(g)** buoyancy frequency squared N^2 and **(h)** turbulent energy dissipation rate ε.

OSD
7, 1439–1467, 2010

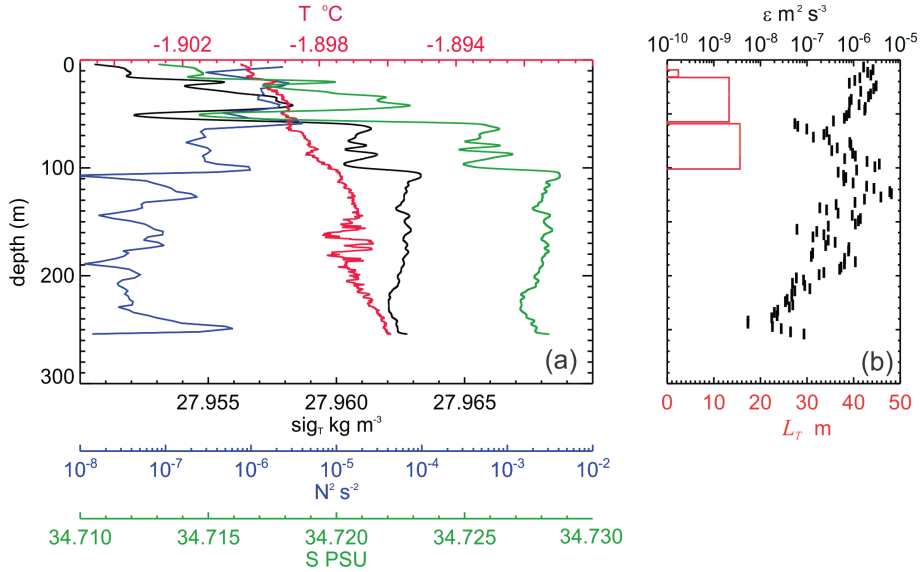

Fig. 4. Single microstructure profile from time=323.95 showing **(a)** temperature, density as σ_t, buoyancy frequency squared N^2 and **(b)** dissipation rate ε and overturning scale L_T.

OSD
7, 1439–1467, 2010

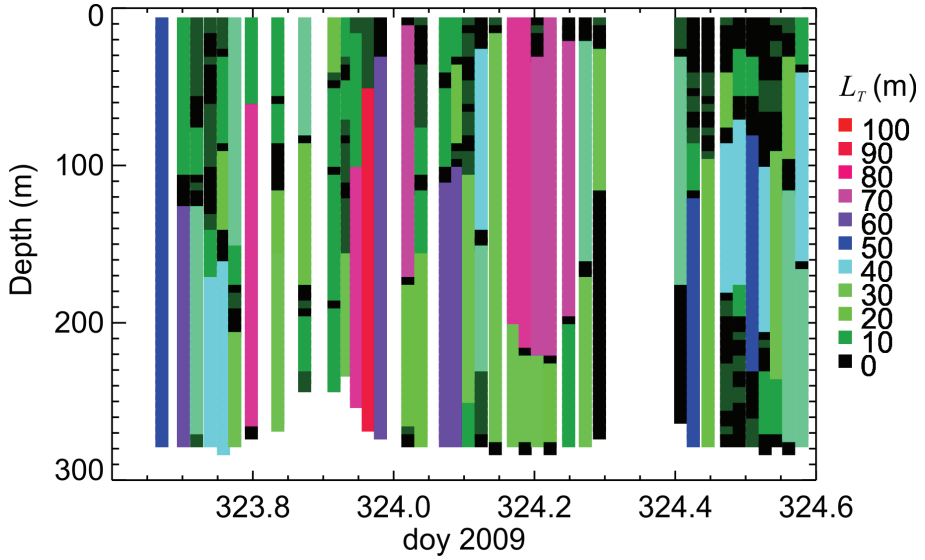

Fig. 5. L_T distribution.

OSD
7, 1439–1467, 2010

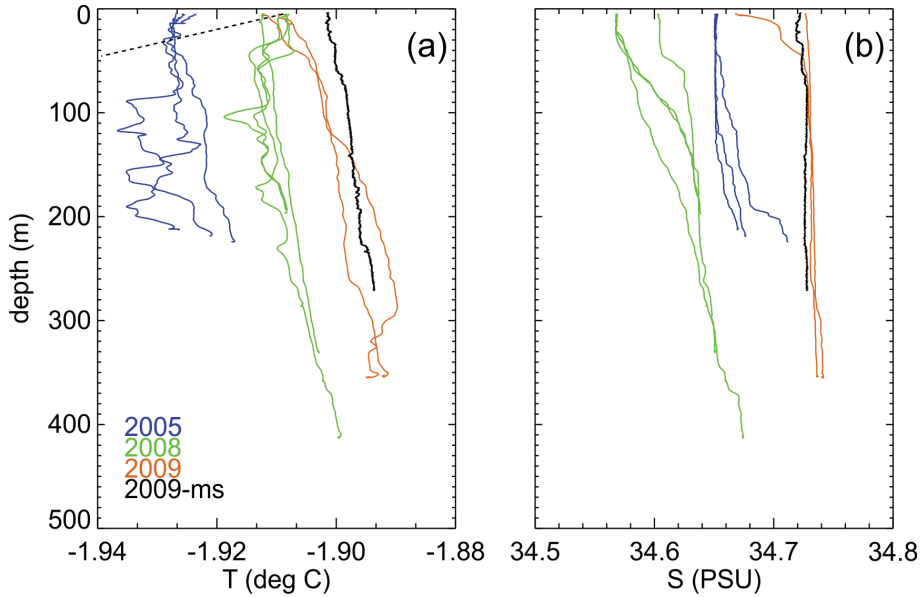

Fig. 6. **(a)** Temperature and **(b)** salinity profile data collected with Seabird Electronics 19+ CTD at various locations within 500 m of the tip of the EGT from the October–November period during 2005, 2008 and 2009, plus a single example from the present microstructure data (2009-ms). The dashed line in the upper part of (a) is the freezing temperature at a nominal salinity of 34.65 PSU. The maximum depth from the 2005 profiles were limited by operational issues. The other profiles all penetrated to within 20 m of the bed indicating the large variation in depth in the region.

OSD
7, 1439–1467, 2010

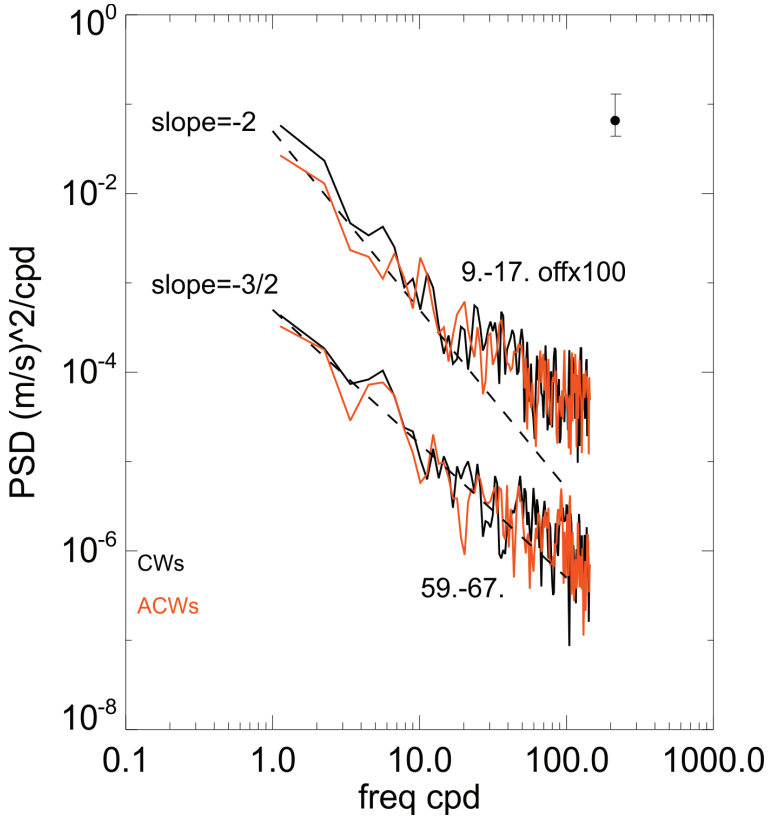

Fig. 7. Rotational spectra of ADCP-derived velocities from depths 9–17 m and 59–67 m. The 95% confidence limit is shown in the top right (Emery and Thomson, 1997). The upper results from shallower depths are offset upwards by two decades. Reference sloped lines are shown with dashes.

OSD
7, 1439–1467, 2010

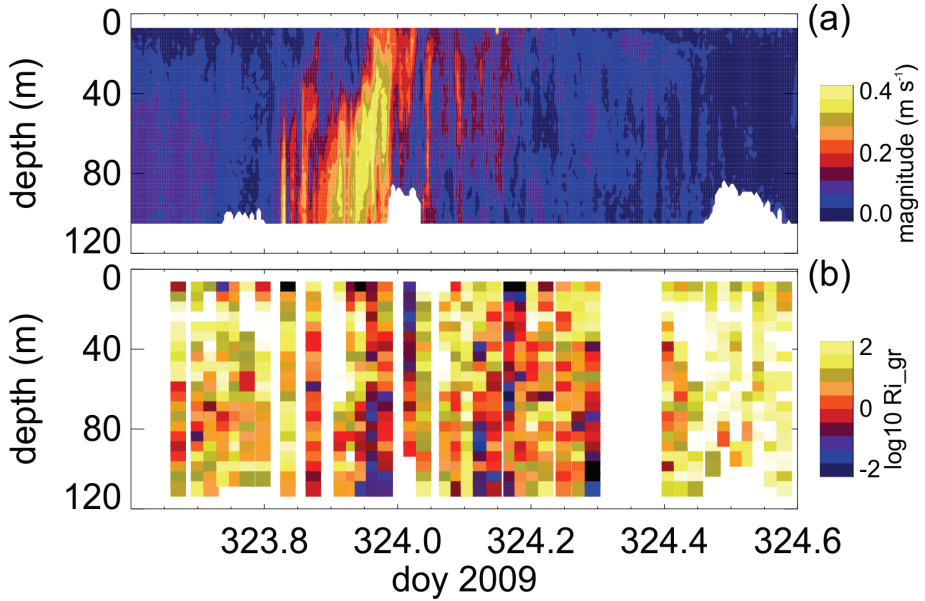

Fig. 8. (a) Velocity magnitude as per Fig. 3a for reference and **(b)** the Ri_{gr} estimate.

OSD
7, 1439–1467, 2010

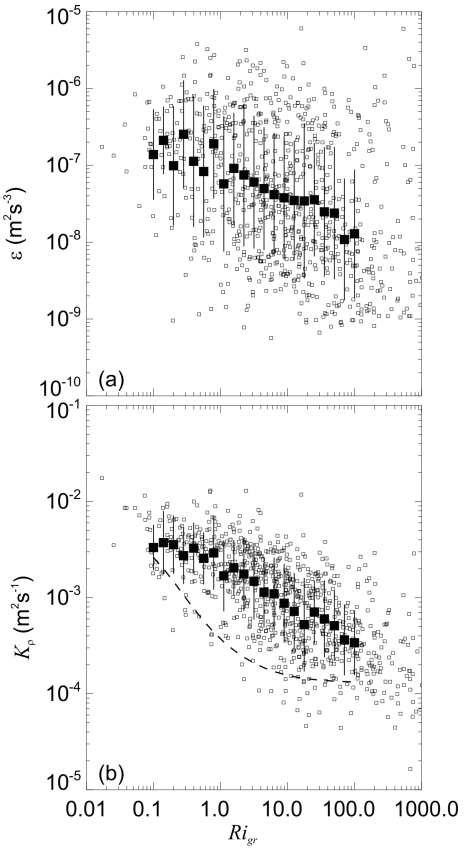

Fig. 9. (a) Dissipation rate as a function of Ri_{gr} showing individual estimates (hollow squares), bin-log-space-averaged (solid squares) and bars showing standard deviation of estimates for 0.15log(Ri_{gr}) spaced bins. **(b)** The same plot format for the diffusivity K_ρ estimate and including the Fer (2006) estimate of vertical diffusivity of mass (dashed line).

OSD
7, 1439–1467, 2010

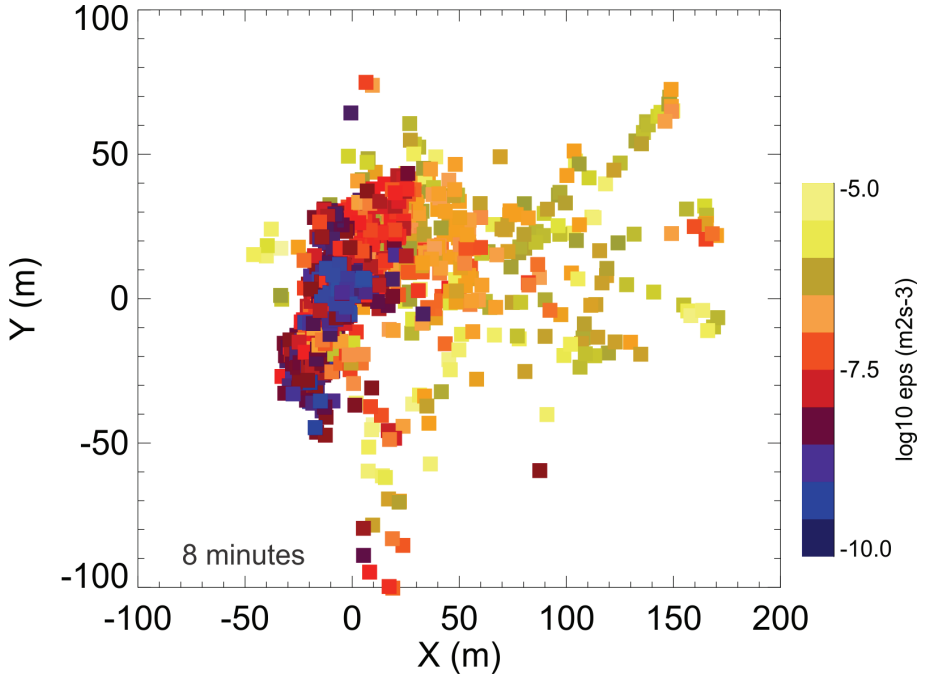

Fig. 10. Dissipation rate as a function of "horizontal displacement" X and Y.

OSD
7, 1439–1467, 2010

Flow and mixing around a glacier tongue

C. L. Stevens et al.

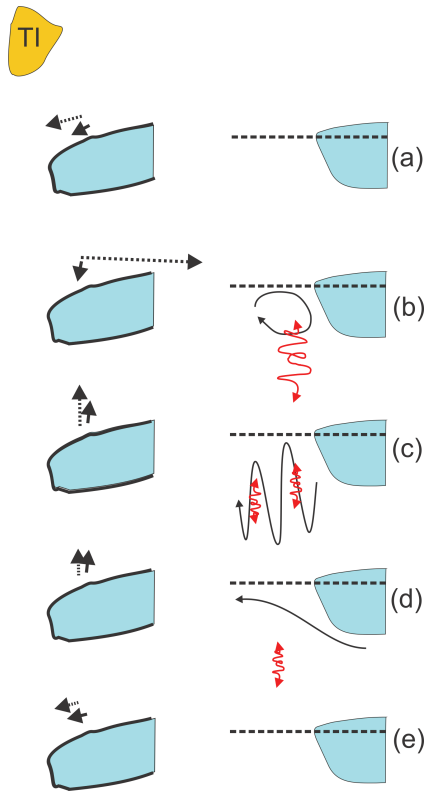

Fig. 11. Interpretive sketches of flow around the tip of the glacier tongue with the left hand panels showing plan view and right hand panels showing elevation view of the north side of the EGT looking to the east. On the left the upper flows (<50 m) are solid and deeper flows dotted. The right hand panels include mixing as red lines. Panels are at approximate times **(a)** 323.7, **(b)** 324.0, **(c)** 324.1, **(d)** 324.3 and **(e)** 324.5. The top panel has Tent Island (TI) for approximate scale and orientation although plan and elevation views are not to the same scale.

OSD
7, 1439–1467, 2010